

White asparagus stem proteins, from waste to interface stabilizer in food foams

Anteun de Groot, Leonard M.C. Sagis, Jack Yang*

Laboratory of Physics and Physical Chemistry of Foods, Wageningen University, Bornse Weiland 9, 6708, WG, Wageningen, the Netherlands

ARTICLE INFO

Keywords:

White asparagus
Waste stream valorization
Protein purification
Interfacial rheology
General stress decomposition
Foams

ABSTRACT

White asparagus stems are a large waste stream that, despite having a high nutritional quality, is currently underutilized. Plant waste stream utilization is often based on extensive processing, which uses copious amounts of resources, and can negatively affect protein functionality. Hence, our study aimed to explore alternative processing routes and characterize the effect of asparagus extract composition on interfacial and foaming properties.

Screw pressing followed by mild purification methods was used to obtain and purify protein extracts from white asparagus stems. Mild purification by filtration removed particles and purification by dialysis removed molecular impurities. Removal of particles and molecular impurities led to improved interfacial properties, as shown with drop tensiometry. The particles disturbed interfacial network formation and the presence of small impurities reduced network density and in-plane interactions. Extracts without particles and molecular impurities formed a dense interface with stiff solid-like behavior and strong in-plane interactions, which resulted in superior foam stability. Additionally, foamability was improved after filtration and/or purification, which could be related to the air bubble size and adsorption rate.

In this study, we identified critical factors for interface and foam stabilizing properties of asparagus proteins, and we revealed the great potential of mildly processed asparagus stem extracts for application in food foams.

1. Introduction

In the last 20 years, the worldwide annual production of green and white asparagus has more than doubled to 17 million tonnes (FOAstat, 2018). Unfortunately, up to 50% of asparagus biomass is considered waste or used for animal feed (Jaramillo-Carmona et al., 2013), which creates a waste stream of up to 8.5 million tonnes. The waste stream mainly consists of leaves and asparagus stems, and utilization would tremendously improve the sustainability of asparagus cultivation. Several studies showed the successful extraction of edible ingredients from waste streams of other plant sources, such as sugar beet leaves and tea leaves, containing respectively 15% and 26.5% (w/w, dry weight) proteins (Finkenstadt, 2014; Ralla et al., 2017; Zhang, Sanders, & Bruins, 2014). Asparagus stems have a comparable protein content of 20% (w/w, dry matter) (Fuentes-Alventosa et al., 2013), showing the potential for protein extraction. Additionally, they contain compounds with high biological value (e.g. phenols and saponins), which can add value to asparagus stem concentrate (Oleszek & Oleszek, 2020; Pegiou et al., 2023; Rodríguez, Jaramillo, Guillén, et al., 2005; Rodríguez,

Jaramillo, Rodríguez, et al., 2005).

Waste valorization through protein extraction usually focuses on separating individual components such as protein, carbohydrates, and oils, but extensive processing can lower protein functionality. Extensive processing is commonly used to extract seed proteins using defatting steps, alkaline extraction and isoelectric point precipitation. This type of processing is costly from an economical and environmental point of view (Apaiah, Linnemann, & Van Der Kooi, 2006; Lie-Piang, Yang, Schutyser, Nikiforidis, & Boom, 2023; van der Goot et al., 2016). A solution could be mild processing of plant-based ingredients, which includes the use of less alkaline extraction pH, omit the isoelectric point precipitation, and the use of diafiltration. For example, mildly processed pea and lupin extracts showed a significantly lower environmental impact per kg extracted protein (Lie-Piang, Braconi, Boom, & van der Padt, 2021). Therefore, this work will focus on the mild extraction of asparagus proteins.

Extensive fractionation often uses heating or pH changes, which can result in a loss of protein functional properties (e.g. foamability) by protein denaturation and subsequent aggregation (Geerts, Nikiforidis,

* Corresponding author.

E-mail address: jack.yang@wur.nl (J. Yang).

<https://doi.org/10.1016/j.foodhyd.2023.109218>

Received 3 May 2023; Received in revised form 22 August 2023; Accepted 25 August 2023

Available online 26 August 2023

0268-005X/© 2023 Published by Elsevier Ltd.

van der Goot, & van der Padt, 2017; L'Hocine, Boye, & Arcand, 2006). This impact on the protein composition and aggregated state can affect the protein adsorption ability at the air-water interface in foams. To obtain stable foams, the proteins need to be able to form stiff viscoelastic layers at the interface, which usually requires native and soluble proteins, instead of heavily aggregated ones (Fruhner, Wantke, & Lunkenheimer, 2000; Martin, Grolle, Bos, Cohen Stuart, & Van Vliet, 2002). Mild protein extraction methods are known to retain the native protein structure, thus avoiding protein aggregation.

A potential risk of milder purification is the presence of more non-proteinaceous material (e.g. small molecular components and cell wall fiber) that can have a high impact on the interfacial functionality of protein. Asparagus contains small molecular components, such as saponins, that can affect proteins on the interface. The most abundant saponin in asparagus is protodioscin (Chitrakar, Zhang, & Adhikari, 2019; Lee, Yoo, & Patil, 2010; M. Wang et al., 2003; Yu, Duan, Yu, & Fan, 2020), which is a steroidal saponin and not surface-active (Góral & Wojciechowski, 2020). A drawback of saponins is their interaction with protein (e.g., with bovine serum albumin) and the possible alteration of the protein structure (Ikeda, Shimoyamada, & Watanabe, 1996; Tanaka, Fang-I, Ishizaki, & Taguchi, 1995). Ultimately, these interactions can change interfacial behavior, thereby changing the foaming properties. Additionally, protein concentrates might still contain cell wall fibers, and it is known that foams can be destabilized by "bridging-dewetting" induced by solid particles (Aveyard & Clint, 1995, 1996; Aveyard, Binks, Fletcher, Peck, & Rutherford, 1994; Frye & Berg, 1989; Garrett, 1979; Roberts, Axberg, & Österlund, 1977). The impact of the cell wall fibers and small molecular components was investigated in this work by systematically removing the non-proteinaceous material using filtration and diafiltration.

In this study, we used a multi-length scale approach to investigate the interface and foam stabilizing potential of several asparagus stem protein extracts. Asparagus stems are screw pressed into a crude juice (CJ), which is filtered into filtered crude juice (FCJ) and purified (filtered and dialyzed) into filtered purified juice (FPJ). In-depth analysis of the nonlinear dilatational rheology was performed with a novel approach, the general stress decomposition method (de Groot, Yang, & Sagis, 2023), which allows for quantitative analysis for the odd and even higher harmonics in the response. The foaming properties were investigated and related to the interfacial characteristics.

2. Material and methods

2.1. Materials

White asparagus stems were kindly provided by Teboza BV (Helden, the Netherlands). Chemical reagents purchased from Sigma-Aldrich or Merck were of analytical grade. Ultrapure water was used for all experiments (MilliQ Purelab Ultra, Germany). All samples were dissolved in a 20 mM phosphate buffer at pH 7, unless stated otherwise.

2.2. Sample preparation

2.2.1. Production of crude juice from asparagus stems

The stems were washed, cut into pieces of 1 cm, and pressed once using a twin-screw press at the fixed speed setting of the device (Angelia 7500, Angel juicer, Netherlands). The juice was filtered over filtration paper, and the filtrate was labelled as crude juice (CJ), which was freeze-dried and stored at -18°C .

2.2.2. Production of purified juice from crude juice

The CJ was further purified by dissolving it in MilliQ water (10%, w/w), followed by centrifugation at $10,000 \times g$ for 30 min. The supernatant was ultrafiltrated (Amicon stirred cell, Merck, USA) with a 5 kDa Ω membrane (Pall Corporation, USA). After 18 h of ultrafiltration, the retentate was dialyzed with a 3.5 kDa standard RC tube (SpectrumLabs,

Greece) for 32 h against demi water. The demi water was replaced 5 times until conductivity was below 1.5 mS/cm. Thereafter, the dialyzed sample was labelled purified juice (PJ), which was freeze-dried and stored at -18°C .

2.2.3. Preparation of protein solutions

CJ and PJ were dissolved based on protein content (dumas) in phosphate buffer for at least 4 h. To investigate the influence of insoluble particles, the samples were filtered with a hydrophilic Millex-GP PES 0.22 μm syringe filter, yielding filtered crude juice (FCJ) and filtered purified juice (FPJ).

2.3. Protein content

The protein content was determined by Dumas and Bradford assay. The Dumas analysis was performed in triplicate by determining the nitrogen content in a flash EA 112 NC Analyzer (Thermo Fischer Scientific INC, USA). Approximately 10 mg of the sample was weighed in tin foil cups, and a nitrogen-to-protein conversion factor of 5.88 was used to calculate the protein content (Urbat, Müller, Hildebrand, Wefers, & Bunzel, 2019). Secondly, a Bradford assay was used to measure 3.5 mg/mL CJ (dry weight) and 1.3 mg/mL PJ (dry weight) in triplicate. CJ and PJ were compared to a BSA calibration curve (0.1–1.4 mg/mL) and a phosphate buffer as a blank. Aliquots of 0.1 mL calibration solution, blank, and sample were added to 3 mL Bradford reagent and carefully mixed. After 30 min, the color development was measured at 595 nm using a spectrophotometer. The efficiency of extraction was compared by calculating the protein recovery (Eq. (1)).

$$\text{Recovery (\%)} = \frac{\text{Total protein in stems (g)}}{\text{Total protein in extract (g)}} * 100 \quad (1)$$

2.4. Protein composition by SDS-PAGE

The protein composition of CJ and PJ was determined by SDS-PAGE (Invitrogen Novex, ThermoFisher Scientific, USA). Protein solutions of 0.1% (w/w) were made in phosphate buffer, and 39 μL sample solution was mixed with 15 μL NuPage™ LDS sample buffer and 6 μL reducing agent (500 mM DDT). Afterwards, the samples were heated at 70°C for 10 min and loaded next to a molecular marker (Mark12™; 2.5–200 kDa) on a 4–12% BisTris gel. The electrophoresis was performed for 30 min at 200 V in MES running buffer, and staining was performed with SimplyBlue™ SafeStain. Hereafter, the stain was washed away with MilliQ, and the gel was stored in a 20% NaCl solution. An image of the gel was made using a gel scanner (GR-900 Calibrated densitometer, Bio-Rad, USA) and analyzed using Image Lab v6.0.1.

2.5. Zeta-potential and particle size

The ζ -potential over a pH range was determined for eight 1.0% CJ (w/w, dry weight) samples at a pH ranging from 2.0 to 9.0 with intervals of 1.0. The samples were centrifuged for 30 min at $10,000 \times g$, and the supernatants were separated from the pellet. The supernatant and pellet were freeze-dried, followed by protein content determination of the fractions by Dumas (see section 2.3). The ζ -potential of the supernatant was measured with a Zetasizer after 10 times dilution in MilliQ (Malvern Instruments Ltd, UK). Particle size distribution of CJ, FCJ, and FPJ, was measured in triplicate at 0.1% protein content (w/w) in phosphate buffer with the Nanosizer (Malvern Instruments Ltd, UK).

2.6. Protein surface hydrophobicity

To determine protein surface hydrophobicity, 8-anilino-1-naphthalenesulfonic acid ammonium salt (ANSa) was used as a fluorescence agent. The protein samples were dissolved in phosphate buffer at a protein concentration range of 0.005–0.04% (w/w). Cuvettes (4 mL

were filled with 3 mL protein solution and 25 μ l of an 8 mM ANSA solution. The cuvettes were carefully rotated to mix the solutions and incubated in the dark for 1 h at room temperature. The fluorescence spectra were measured using an LS 50B luminescence spectrometer (PerkinElmer, USA) at an excitation and emission wavelength of 390 nm and 470 nm (slit width 5 nm), respectively. A phosphate buffer solution with ANSA was included as a blank. The slope of the fluorescence intensity versus the protein concentration was determined as the protein surface hydrophobicity.

2.7. Determination of surface tension and surface dilatational properties

The air-water surface dilatational properties were determined with a drop tensiometer PAT-1M 1D (Sinterface Technologies, Germany). A hanging drop with a surface area of 20 mm² was formed at the tip of the needle. By fitting the droplet profile to the Young-Laplace equation, the surface tension was calculated. The surface tension was monitored for 10,800 s, which was followed by oscillatory dilatational deformations of the interface, an amplitude or a frequency sweep. In the amplitude sweep, the deformation amplitude was varied between 0.05 and 0.3 at a frequency of 0.02 Hz. During a frequency sweep, the amplitude was fixed at 0.03, and the frequency was varied between 0.005 and 0.1 Hz. In these measurements, five sinusoidal oscillations were performed at each amplitude and frequency. All measurements were performed at least in triplicate at room temperature.

We did not measure the time evolution of the dilatational moduli. A prerequisite to measuring this is that the measurement can be performed in the LVE regime. In general, that kind of test works well for low molecular weight surfactant systems, for which the response is relatively insensitive to strain amplitude. However, protein-stabilized interfaces tend to have a very low maximum linear strain, which is often below the minimum amplitude we can still apply in commercial tensiometers and get reliable results. For this reason, oscillations during the adsorption phase were not applied, since it would affect the structure of the protein film.

2.8. Analysis of surface dilatational data

The amplitude sweeps in oscillatory dilatation were studied using Lissajous plots. The plots are created by plotting the surface pressure ($\Pi = \gamma - \gamma_0$) versus the deformation $((A - A_0)/A_0)$. Here, γ and A are the surface tension and area of the deformed interface, γ_0 and A_0 are the surface tension and area of the non-deformed interface. The plots were constructed from the middle three cycles for each deformation.

Recently the nature of nonlinearities emerging in dilatational rheology was described and quantified by splitting the harmonics into odd and even harmonics (de Groot et al., 2023). In that work, it was shown that odd harmonics describe the network properties of the interface, and even harmonics describe surface density changes. Network properties relate to in-plane interactions between the particles and describe the response of the protein network to stretching and compression, and surface density changes result from the changes in the number of molecules per unit area during compression and expansion. Both have fundamentally different responses to the applied strain resulting in a split into odd and even harmonics.

Upon deformations of the form $\varepsilon = \varepsilon_0 \sin(\omega t)$, the dilatational stress response, is described by Eq. (2).

$$\Pi(t) = \sum_{n=0}^6 q_n \sin(n\omega t + \delta_n) \quad (2)$$

where ε_0 is the strain amplitude, ω is the frequency of oscillation, and t is time. The resulting stress response, $\Pi(t)$, in Eq. (2) is analyzed up to the 6th harmonic (n) with phase shift, δ_n . For our analysis, the stress in Eq. (2) was split into the four individual components, corresponding to the odd and even sine and cosine functions given by Eq. 3 – Eq. (6):

$$\tau_1 = \sum_{k=0}^2 b'_{2k+1} \sin((2k+1)\omega t) \quad (3)$$

$$\tau_2 = \sum_{k=0}^2 a'_{2k+1} \cos((2k+1)\omega t) \quad (4)$$

$$\tau_3 = \sum_{k=0}^3 c'_{2k} \sin(2k\omega t) \quad (5)$$

$$\tau_4 = \sum_{k=0}^3 d'_{2k} \cos(2k\omega t) \quad (6)$$

Here, a'_{2k+1} , b'_{2k+1} , c'_{2k} , d'_{2k} are the coefficients of each harmonic with the subscript indicating which harmonic it is. Notice that n is replaced by k to describe each set of harmonics.

To analyze the contribution of higher harmonics, a MATLAB (R2020b) script based on the previously mentioned work was used (de Groot et al., 2023). This script creates a smoothed stress signal to decrease the noise and improve analysis. First, the middle 3 oscillations of the strain and stress are interpolated over one period. Thereafter, a fast Fourier transformation is performed from which the components $\tau_1 - \tau_4$ and a reconstructed signal were calculated based on the first six harmonics. The individual stress components are plotted in Lissajous plots and quantified using Eq. 7 – Eq. (13):

$$E_{\tau 1L} = \frac{\sum_{k=0}^2 b'_{2k+1} (-1)^k}{\varepsilon_0} \quad (7)$$

$$E_{\tau 1M} = \frac{\sum_{k=0}^2 (2k+1) b'_{2k+1}}{\varepsilon_0} \quad (8)$$

$$S = \frac{E_{\tau 1L} - E_{\tau 1M}}{E_{\tau 1L}} \quad (9)$$

$$E_{\tau 4} = -\frac{\sum_{k=0}^2 2d'_{4k+2}}{\varepsilon_0} \quad (10)$$

$$\gamma_s = d'_0 \quad (11)$$

$$U_{d\tau 2} = \pi \varepsilon_0^2 E_1^* \quad (12)$$

$$U_{d\tau 3} = 2\varepsilon_0^2 \sum_{k=1}^3 \left(\frac{E_{2k\tau 3} * k}{k^2 - 1/4} \right) \quad (13)$$

In these expressions $E_{\tau 1L}$ is the elastic modulus at large intra-cycle deformation for the odd harmonics $E_{\tau 1M}$ is the elastic modulus at zero intra-cycle strain for the odd harmonics; both moduli are used to calculate the intracycle strain hardening factor, S . The dissipated energy for the odd harmonics $U_{d\tau 2}$ is calculated from the loss modulus of the first harmonic, E_1^* . For the even harmonics, the modulus and dissipated energy are described by, $E_{\tau 4}$ and $U_{d\tau 3}$, where $E_{2k\tau 3}$ is the corresponding modulus of each harmonic contained in τ_3 ; finally, γ_s denotes the overall vertical shift of the signal from the even harmonics. For a graphical interpretation of these parameters, we refer to the study of (de Groot et al., 2023).

2.9. Foam characteristics

Foaming properties were determined at a protein concentration of 0.1% (w/w) in a phosphate buffer. Foam formation with whipping was done in plastic tubes with 34 mm diameter, which was filled with 15 mL

solution. The solutions were stirred at 2000 rpm with an overhead stirrer (RW 20 digital, IKA, Germany) for 2 min. Initial foam height was recorded by measuring the distance from the bottom to the top of the foam. The content in the tube was poured into a 50 mL glass cylinder, and the foam and liquid height were recorded. The overrun is calculated by the foam volume divided by the initial solution volume (15 mL). This experiment was performed at least in duplicate at room temperature.

Foaming properties upon sparging were measured with a Foamscan (Teclis IT-Concept, France) foaming device. Nitrogen gas is sparged through a metal frit (27 μm pore size, 100 μm distance between centers of pores, square lattice). A total 40 mL solution was sparged in a glass cylinder (\varnothing 60 mm) at a 400 mL/min gas flow rate to a maximal foam volume of 400 cm^3 . A camera and Foamscan software monitored the foam decay until it reached a foam volume of 200 cm^3 . Another SLR camera took a picture of the bubbles every second, these were used for bubble size analysis with DIPlip and DIPimage in MATLAB. As a measure for foamability, the time needed to form 400 cm^3 foam was used, whereas the foam half-life time was used to indicate foam stability.

2.10. Statistical analysis

A two-tailed student's t-test was performed with equal variance to identify significant differences. A difference was considered significant at $p < 0.05$. When a student's t-test was performed this is explicitly mentioned as significantly different.

3. Results & discussion

3.1. Composition

Asparagus stems are not a well-studied protein source. Hence we will first determine the composition of the protein extracts. The extraction of crude juice (CJ) from asparagus stems yielded an extract with 19.9% (w/w) protein and a protein recovery of 60.5%. Subsequently, CJ was purified by centrifugation and dialysis. The purified juice (PJ) had a protein content of 53.8% (w/w) and a protein recovery of 6.2%, as measured with dumas. Dumas measures all protein, and we are interested in the soluble part. Hence, we also determined the protein content of CJ and PJ with a Bradford assay. The assay showed a soluble protein content of 2.9% (w/w) for CJ and 25.7% (w/w) for PJ, which points to a large part of the proteins being insoluble.

Plant protein extract can contain significant amounts of aggregated protein (Yang, Mocking-Bode, et al., 2022). In plants protein extracts, part of the protein is insoluble because of heavy glycosylation and/or embedding in cell-matrix polymers. Hence we measured the size distribution of CJ, filtered CJ (FCJ), and filtered PJ (FPJ) in Fig. 1. Here, CJ shows the presence of large particle with a peak at 1100 nm, which shifts to lower sizes for FCJ and FPJ. FPJ has a bimodal peak distribution with peaks at 40 and at 400 nm. The latter is most likely a small fraction of

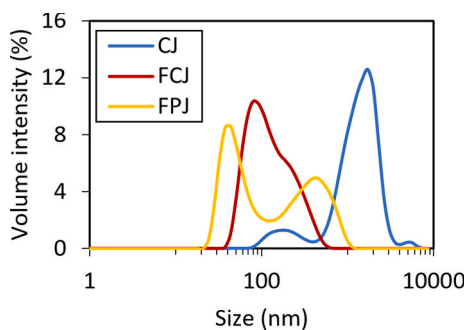


Fig. 1. The particle size distribution of CJ (blue), FCJ (red), and FPJ (yellow). The measurement was performed in triplicate, here one representative graph is shown per sample.

aggregates which we could not completely remove from the sample. However, it should be noted that the distribution is volume-based, and the peaks differ by a factor of 10. A volume-based distribution is weighted by R^3 , hence on a number basis, the height of the second peak would reduce by a factor 1000; so most of the particles here are given by the first peak. Therefore we conclude that the large particles present in CJ were removed upon filtration and purification.

3.2. Protein properties

Protein composition can have a big effect on the interfacial functionality, hence we determined protein size with SDS-PAGE. The results in Fig. 2 show similar band patterns for CJ and PJ, pointing towards a similar protein composition of CJ and PJ. Identifying individual bands is challenging as studies on protein composition of asparagus are very limited. Composition analysis in more general terms is still possible by comparing it to other plant protein concentrates. In a comparative study on pea and bean proteins, globulins were identified in the \sim 40–70 kDa range, with their subunits at \sim 20–40 kDa (Yang, Kornet, et al., 2022). Albumins are generally smaller and were identified at \sim 20–30 kDa with subunits below \sim 20 kDa (Yang, Kornet, et al., 2022). Soy protein globulins and their subunits span a similar range of molecular weights (Wang et al., 2022). The three bands at the top of the gel are probably a mixture of globulin and albumin; These bands were found in both albumin and globulin fractions of mung bean, Bambara groundnut, and pea (Yang, Kornet, et al., 2022). Comparing these results with literature gives a better idea of how asparagus protein compares to other plant proteins and suggests that our asparagus protein concentrates consist of a combination of globulin and albumin.

Further characterization of CJ was performed by measuring its zeta-potential at pH 2–9, (Fig. 3). The isoelectric point is estimated to be around pH 3.7, which is relatively low compared to other globulins, where the isoelectric point is generally pH 4–5 (Derbyshire, Wright, & Boulter, 1976; Karaca, Low, & Nickerson, 2011; Shevkani, Singh, Kaur, & Rana, 2015).

Protein surface hydrophobicity was measured with 8-Anilino-1-naphthalenesulfonic acid (ANSA) at protein concentrations of 0.005–0.04% (w/w). CJ had a relative surface hydrophobicity of 0.36 compared to PJ.

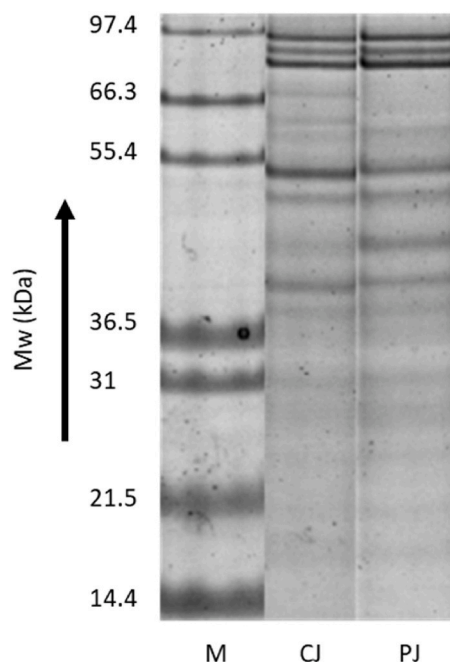


Fig. 2. SDS-PAGE gel scan under reducing conditions with a molecular marker, (M), CJ (0.8%, w/w), and PJ (0.1%, w/w).

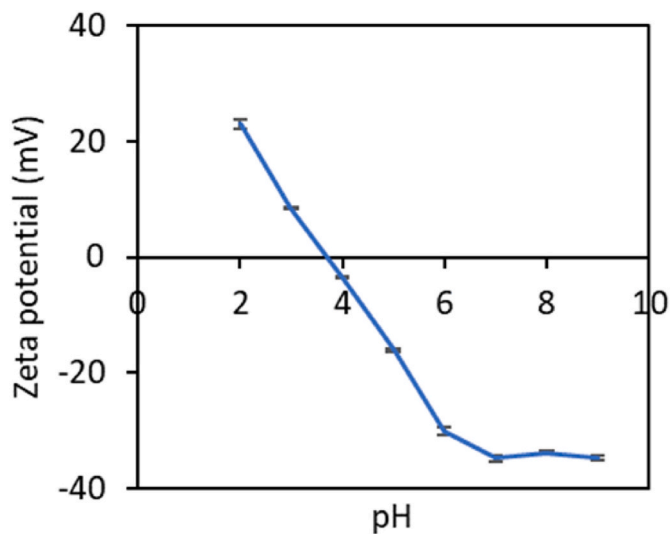


Fig. 3. Zeta-potential as a function of pH of 0.1% CJ (w/w). This experiment was performed in triplicate.

The processing was not expected to alter the protein structure since centrifugation, ultrafiltration and dialysis were used to purify the CJ. However, small molecular components present in CJ (e.g., phenolic compounds and/or saponins) can interact with the protein, effectively shielding hydrophobic patches on the surface. Phenolic compounds are known to alter protein structure (Ozdal, Capanoglu, & Altay, 2013), possibly resulting in lower surface hydrophobicity. Also, saponins are shown to have interactions with proteins and can alter their structure (Ikeda et al., 1996; Tanaka et al., 1995), potentially lowering surface hydrophobicity.

3.3. Adsorption behavior

The interfacial properties of crude juice (CJ), filtered crude juice (FCJ), and filtered purified juice (FPJ) were studied using droplet tensiometry. The adsorption behavior of each extract was measured for 3 h (Fig. 4), reaching surface pressures of around 25 mN/m. This total increase in surface pressure is similar to the increase seen in other plant proteins. Soy and pea protein isolates also reached a surface pressure of

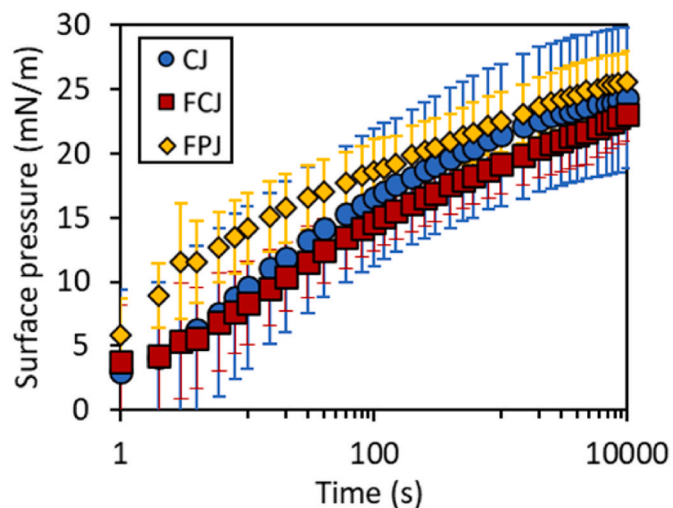


Fig. 4. Surface pressure over time of CJ (blue circles), FCJ (red squares), and FPJ (yellow diamonds). All samples are dissolved at a concentration of 0.1% (w/w) protein. Average surface pressure of at least seven measurements is shown, including standard deviation.

around 25 mN/m at similar concentrations (Martínez, Carrera Sánchez, Rodríguez Patino, & Pilosof, 2009; Mohanan, Nickerson, & Ghosh, 2020).

During the first 20 s, FPJ-stabilized interfaces showed a significantly higher surface pressure than CJ- and FCJ-stabilized interfaces. A higher surface pressure in the initial phase indicates a higher adsorption rate for FPJ, which could be because of the increased surface hydrophobicity of PJ. Proteins with a higher hydrophobicity have a lower energy barrier for adsorption on the air-water interface, especially in the initial stage (Wierenga, Meinders, Egmond, Voragen, & De Jongh, 2003). Alternatively, the increased soluble protein content in PJ could also result in faster adsorption to the interface, as adsorption rate increases with increasing protein bulk concentrations (Mitropoulos, Mütze, & Fischer, 2014).

After 1000 s, the increase in surface pressure is much slower, which is seen for many protein-stabilized interfaces. Most proteins tend to form disordered viscoelastic solid interfaces, through changing their structural conformation at and interface by reorienting their hydrophobic and hydrophilic regions. The extent and reversibility of structural rearrangements depend on the type of protein (Clarkson, Cui, & Darton, 1999) and on the polarity of the non-aqueous phase (Bergfreund, Bertsch, & Fischer, 2021). Through non-covalent intermolecular interactions proteins can form a stiff viscoelastic interface (Bos & Van Vliet, 2001; Clarkson et al., 1999) with a wide range of relaxation times, essentially forming non-equilibrium systems (Sagis et al., 2019). Therefore, the slow surface pressure increase is related to long-term protein rearrangements at the interface through conformational changes of the proteins and/or in-plane clustering of the proteins (Richtering, 2012; Rühs, Affolter, Windhab, & Fischer, 2013; Sagis et al., 2019). Hence, performing oscillatory dilatation experiments in equilibrium is impossible, but letting the interface equilibrate for 3 h can ensure a quasi-steady state.

3.4. Surface oscillatory dilatational rheology

3.4.1. Frequency sweep

After adsorption, the asparagus stem protein-stabilized interfaces were subjected to frequency sweeps, and the results are presented in Fig. 5 A. All asparagus protein-stabilized interfaces show a higher dilatational storage modulus, E_d' , compared to the loss modulus, E_d'' (data not shown). This reveals a predominantly elastic interface over the range of frequencies studied here. Within this range, the storage modulus showed a power law dependence on frequency ω . This dependence was quantified by fitting $E_d' \sim \omega^n$, yielding exponents of 0.22 (± 0.03), 0.15 (± 0.04), and 0.21 (± 0.03) for respectively CJ, FCJ, and FPJ-stabilized interfaces.

According to the Lucassen-van den Tempel model, an exponent of 0.5 is typically seen for low molecular weight surfactants with limited in-plane interactions, where the surface elasticity is dominated by the exchange between the bulk and interface (Lucassen & Van Den Tempel, 1972). A slope of around 0.1 suggests disordered solid behavior (either a jammed or gelled interface), with a broad relaxation spectrum. Typically, other processes dominate the elastic response, such as in-plane interactions or momentum transfer between the bulk and interface (Sagis et al., 2019). The observed exponents suggest that the proteins in all fractions self-assemble into disordered solid structures after adsorption, with a negligible effect of mass transfer between bulk and interface on elasticity.

Interestingly, FCJ has a significantly lower exponent than CJ, indicating an effect of insoluble particles in CJ. The insoluble particles apparently affect network formation, leading to a somewhat stronger frequency dependence and a higher stiffness for FCJ. We will further explore the effect of insoluble particles and molecular impurities in the next section, where we analyze dilatational amplitude sweeps.

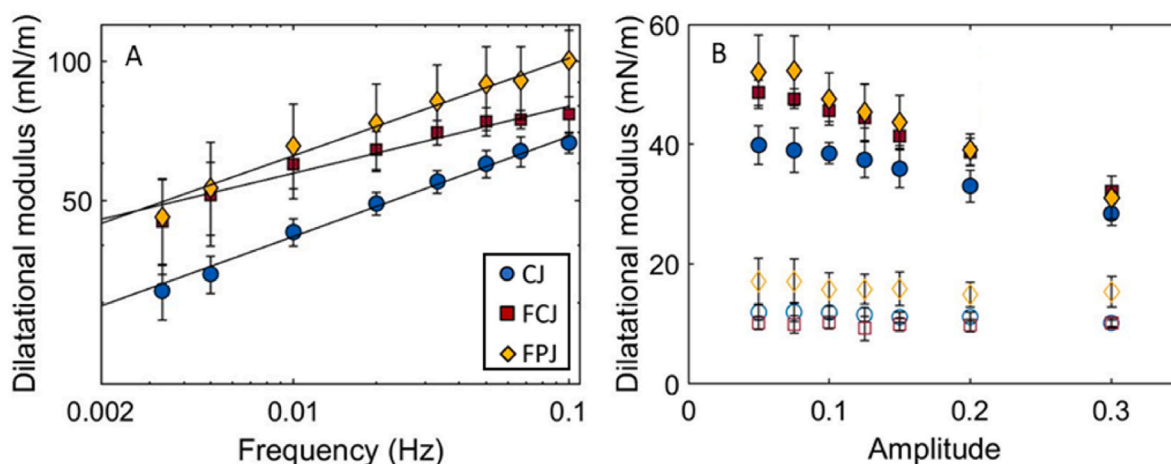


Fig. 5. The dilatational moduli plotted versus the frequency and amplitude in plot A and B, respectively. With CJ (blue circles), FCJ (red squares), and FPJ (yellow diamonds) in a 20 mM PO_4 buffer at pH 7. The closed symbols correspond to E_d' , and the open symbols E_d'' . Both experiments are measured at least in triplicate.

3.4.2. Amplitude sweep

The mechanical properties of the interfacial films were studied with amplitude sweeps, and the results are shown in Fig. 5 B. During the amplitude sweep, E_d'' is consistently lower than E_d' , indicating an elastic interface is formed for all samples. CJ-stabilized interfaces have a lower stiffness ($E_d' = 40$ mN/m) at small amplitudes compared to FCJ-, and FPJ-stabilized interfaces ($E_d' = 49$ mN/m and $E_d' = 52$). Upon increasing amplitude, all interfaces show a decreasing elastic modulus. The decrease is a result of an increased disruption of the interfacial microstructure. Typically, this is seen for proteins that form a viscoelastic solid layer at the interface (Van Kempen, Schols, Van Der Linden, & Sagis, 2013). Increasing the strain amplitude to 0.3, the elastic modulus of CJ decreased by 14 mN/m, of FCJ by 16 mN/m, and FPJ-stabilized interfaces decreased by 20 mN/m. Hence, the effects of the disruption of the interfacial microstructure are most pronounced in FPJ-stabilized interfaces. The breakdown of interfacial microstructure introduces higher harmonics to the system, and only using a first harmonic modulus gives an incomplete representation of the actual response (de Groot et al., 2023). Hence, we examined the nonlinear behavior in more detail using Lissajous plots (Erni & Parker, 2012; Van Kempen et al., 2013).

3.4.3. Lissajous plots

Lissajous plots were constructed by plotting the surface pressure against deformation. In these plots, the cycle is clockwise, and expansion starts at the bottom left and ends at the upper right corner (i.e., the upper

part of the loop); the compression phase of the cycle goes from the upper right to the lower left corner (See Fig. 6 C).

At small deformations, the Lissajous plots are symmetric, indicating linear viscoelastic behavior (Fig. 6 A). Here, the first harmonic modulus is a good representation of the intracycle behavior. The cycle for CJ is tilted more towards the horizontal axis compared to FCJ, and FPJ which corresponds to a lower elastic modulus. CJ displays a relatively linear viscoelastic elastic response over the whole amplitude sweep, even at 0.3, the response for expansion and compression are almost the same. In contrast, FCJ and FPJ show a nonlinear response at 0.3 deformation. Here, the intracycle behavior cannot be described only as a modulus based on the first harmonic (E_d'), as the expansion response differs from compression. For example, FPJ at 0.3 deformation shows an initial steep response at the beginning of the expansion, but the slope decreases to almost zero at maximum expansion, whereas in compression, the response is a straight line. The nature of this nonlinear asymmetric response can be analyzed and quantified in more detail using the recently developed general stress decomposition method (de Groot et al., 2023), as we will show in the next section.

3.4.4. Stress decomposition

Quantifying the nonlinearities by decomposing the stress will give more insights into the mechanical properties of the interface. The stress decomposition is based on splitting the odd and even harmonics of the Fourier-transformed stress signal. The odd harmonics are related to the network properties of the interface and can be split into an elastic and

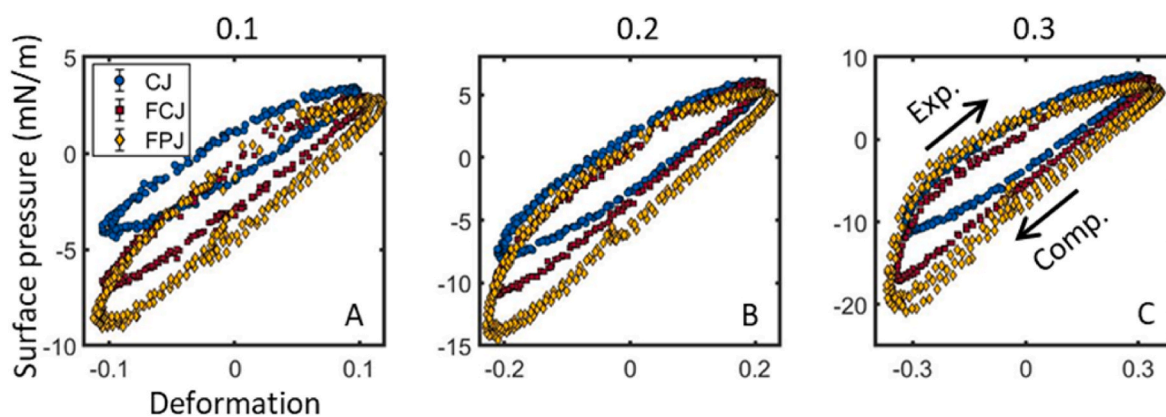


Fig. 6. Lissajous plots of surface pressure against deformation for the amplitudes: 0.1, 0.2, and 0.3. The blue circles correspond to CJ, red squares to FCJ, yellow diamonds to FPJ. All samples are dissolved in 20 mM PO_4 buffer at pH 7 and 0.1% (w/w) protein and at least measured in triplicate of which one representative sample is displayed here.

viscous contribution, respectively τ_1 & τ_2 ; The even harmonics are related to changes in surface density during oscillations introduced by the nonlinearities in the surface-pressure area isotherm and consist of a dissipative and elastic contribution, respectively τ_3 & τ_4 (de Groot et al., 2023).

Decomposition offers an interpretation of the Lissajous plots (Fig. 7), and quantification in the form of various parameters describing the interfacial response (Fig. 8). In Fig. 7, we see increasing nonlinearities from CJ to FPJ, which are quantified in Fig. 8.

The modulus $E_{\tau_{1L}}$ is plotted versus the deformation amplitude in Fig. 8 A. All interfaces show a decreasing network stiffness with increasing deformations, indicating a breakdown of the interfacial microstructure at increasing deformations. Here, we see that FCJ and FPJ form a stiffer network than CJ, as $E_{\tau_{1L}}$ is significantly higher for these fraction than for CJ. The removal of particles in FCJ increased the interfacial stiffness, hereby confirming the observations in the frequency sweep that particles are affecting network formation at the interface. Additional removal of molecular impurities (FPJ) did not increase the network stiffness significantly.

The microstructural breakdown with increasing amplitude results in an S-factor significantly lower than 0 for CJ at 0.3 strain (Fig. 8 B), which indicates strain softening. Contrarily, FPJ had an S-factor significantly higher than 0, indicating strain hardening. The strain hardening in FPJ indicates the stretching of residual network clusters, whereas the strain softening shows a breakdown of the structure in the CJ-stabilized interfaces, which starts flowing. FCJ showed no significant strain hardening or softening, indicating that the removal of particles resulted in a decrease of structure breakdown at the extremes of deformation, compared to CJ.

FPJ-stabilized interfaces show a wider plot for $\tau_1 + \tau_2$ and $\tau_3 + \tau_4$ in Fig. 7 H and J. The total area of a Lissajous plot shows the total dissipated energy per cycle, and is calculated with $U_{d\tau_2}$ and $U_{d\tau_3}$ (Eqs. (12) and (13)). In Fig. 8 E & F, FPJ shows relatively high values for U_{τ_2} and U_{τ_3} , which indicates stronger in-plane interactions.

Large deformations (>0.1) result in a more negative value for E_{τ_4} for

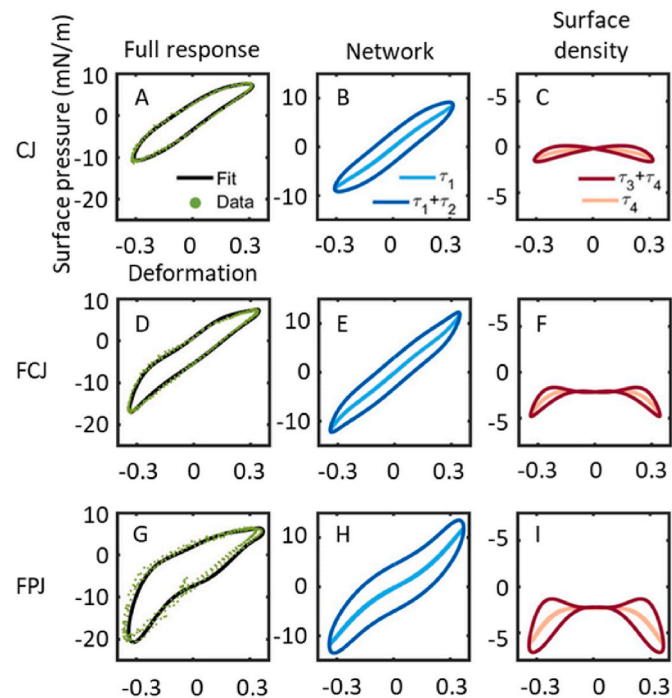


Fig. 7. The Lissajous plot from decomposition of CJ, FCJ, and FPJ at 0.3 deformation. With the raw data (green, dots) and the fitted response (black, line) plotted in plot A, D, G, τ_1 (light blue) and $\tau_1 + \tau_2$ (blue) in plot B, E, H and τ_4 (light red) and $\tau_3 + \tau_4$ (red) in plot C, F, I.

FPJ compared to CJ and FCJ (Fig. 8 C). When density changes have a more important contribution to the total surface stress, this indicates a more densely packed interface with limited bulk-interface exchange (as shown in the frequency sweeps) and strong in-plane interactions. Hence, we conclude that FPJ forms a denser interfacial film with stronger in-plane interactions, compared to CJ and FCJ.

Higher network stiffness, in combination with higher surface density, will reduce in-plane mobility. This is reflected by the shift (γ_s , Fig. 8 D), which is large for FPJ, indicating deformations around a dynamic state far from the surface pressure-area isotherm. Since the in-plane relaxations are slow, FPJ-stabilized interfaces are not able to restore themselves quickly enough to return to the equilibrium state at zero deformation.

In conclusion, CJ-stabilized interfaces had the weakest interface indicating weak in-plane interactions, and showed intracycle strain softening. The interface of CJ is affected by particles and molecular impurities, and filtration, which removed particles in FCJ resulted in a stiffer network with no significant strain softening. Additional purification removed molecular impurities leading to the formation of a dense and stiff interfacial network with strong in-plane interactions for FPJ.

Possible mechanisms for the effects of insoluble particles and molecular impurities are that they co-adsorb to the interface or interact with the adsorbed protein in a sublayer of the interface. In this way, they both affect in-plane protein-protein interactions within the interface. However, more research should be done to determine the exact mechanisms of interfacial network disruption by the impurities and insoluble particles.

3.5. Foams

Asparagus protein-stabilized foams were studied for their foamability, foam stability and air bubble size after sparging, and foamability after whipping. The foamability in sparging was measured as the time required to reach a foam volume of 400 cm³ (Fig. 9 A). This figure shows that FCJ-, and FPJ-stabilized foams were formed within 114 ± 11, and 80 ± 2 s, whereas CJ did not reach 400 cm³ foam. With whipping, a similar trend is shown; CJ had the lowest foam overrun, FCJ was 5x higher, and FPJ was even 7x higher than CJ (Fig. 9 B). Hence, particles in CJ again hampered the foam formation, which was improved with filtration in FCJ and additional removal of molecular components in FPJ.

The absence of a CJ-stabilized foam in sparging was unexpected, since it reduced surface tension similarly to FCJ. Hence, we expect that particles in CJ had an anti-foaming effect during sparging. Anti-foaming occurs through bridge-dewetting: due to the hydrophobic nature of the particles the water within foam lamellae will be repelled, decreasing the lamellae thickness until rupture. Even though we expect hydrophilic particles (contact angle <90°) in the extract, we still expect bridge-dewetting because they are likely to be irregularly shaped. It has been shown that irregular hydrophilic particles, with contact angles as low as 40°, can have a significant anti-foaming effect (Denkov, Marinova, & Tcholakova, 2014; Frye & Berg, 1989; Garrett, 1979).

In sparging, the rate and extent to which the protein can lower the surface tension strongly affect the air bubble size. A faster rate and greater extent of reduction will result in smaller initial air bubbles (Bolontrade, Scilingo, & Añón, 2013; Kawale, van Nimwegen, Portela, van Dijk, & Henkes, 2015). The surface tension reduction during the first 10 s of protein adsorption in Fig. 4 was significantly faster for FPJ, which resulted in smaller bubbles and faster foam formation during sparging compared to CJ and FCJ in Fig. 9 A, representative pictures of FCJ and FPJ foams are shown in the supplementary information (Fig. S11). This is in agreement with the trend that emerges in foam formation, that high foamability (e.g. low foam formation time) corresponds to small air bubbles.

It is interesting to compare foam whipping properties of asparagus stem proteins with other plant proteins reported in literature. Other

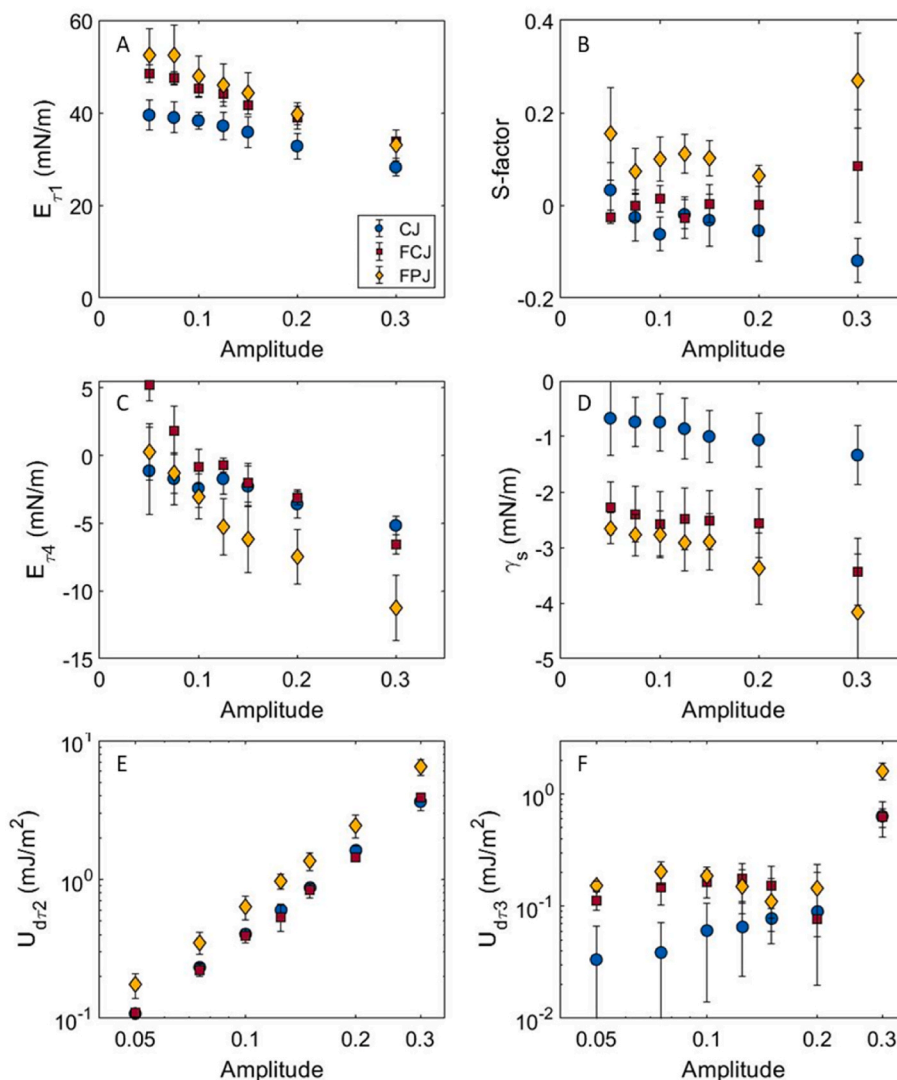


Fig. 8. The stress decomposition of dilatational amplitude sweep into $E_{\tau 1L}$ (A), S-factor (B), $E_{\tau 4}$ (C), shift γ_s (D), U_{dr2} (E), and U_{dr3} (F) plotted over the range of deformations applied in the strain sweep for air-water interfaces stabilized by CJ (blue, circles), FCJ (red, squares), and FPJ (yellow, diamonds).

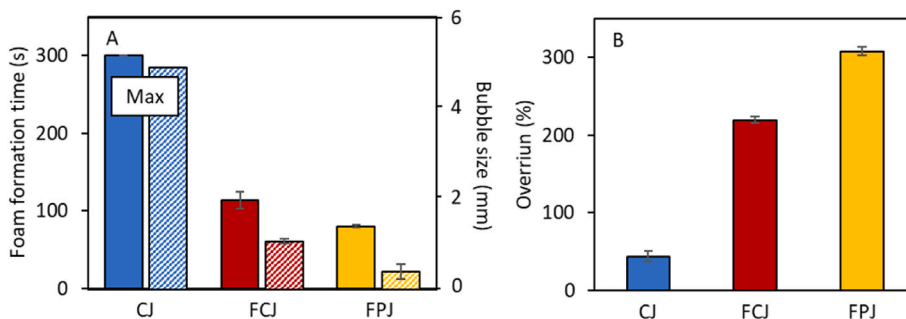


Fig. 9. Plot A shows the time needed to form 400 cm³ foam from 50 mL 0.1% w/w protein solution during sparging on the left axis, and on the right axis the bubble radius. Bars with solid colors display sparging foam formation times and the striped bars show bubble size. CJ had a foam formation time and bubble size higher than the detection limit as indicated by 'max'. In plot B, the foam overrun for 2 min at 2000 rpm at 0.1% w/w protein. With CJ (blue), FCJ (red), and FPJ (yellow).

plant protein stabilized foams show overrun values of 100%, 400%, and 333% for respectively soy protein, pea protein, and alfalfa protein when prepared by whipping (Lamsal, Koegel, & Gunasekaran, 2007; Lamsal et al., 2007; Martínez et al., 2009; Mohanan et al., 2020; Mohanan et al., 2020). The asparagus stem extract foams perform similar to other plant proteins, as FPJ had a higher overrun than soy protein and similar

overrun to pea and alfalfa but at lower concentrations.

The foam stability of the asparagus protein-stabilized interfaces was measured after sparging. After sparging the foam to 400 cm³, the time required for the volume to decrease to 200 cm³ was recorded (foam half-life time) and used as a measure for foam stability. CJ did not reach the required foam height, so it is highly unstable. The foam half-life time of

FCJ (227 s) was low compared to FPJ (2528 s) as shown in Fig. 10. A 10-fold increase in foam stability of FPJ compared to FCJ signifies the importance of interfacial properties for foam stability. FPJ-stabilized interfaces form a stiff and dense viscoelastic layer with strong in-plane interactions, which results in a greatly improved foam stability compared to CJ and FCJ.

Comparing our results to literature we find that the foamability of FCJ and FPJ are comparable to the albumin-rich fractions of mungbean, Bambara groundnut, and pea (Yang, Kornet, et al., 2022). Here, the researchers, using the same foaming method, showed that albumins adsorb faster and form more stable foams than globulins. However, the foam half-life time (foam stability) of FPJ is comparable to the globulin fractions of mungbean, Bambara groundnut, and pea (Yang, Kornet, et al., 2022). Apparently, both fractions are adsorbing to the interface for FPJ, and stability is dominated by the globulins.

4. Conclusions

In this study, we assessed the effect of molecular impurities and particles on the functionality of asparagus stem proteins. Proteins were extracted from asparagus stems, which are normally regarded as waste, followed by increasing levels of purification. Crude juice was produced by screw pressing the asparagus stems. The crude juice was compared to a filtered extract (to remove particles) and a filtered and dialyzed extract (to remove particles and molecular impurities).

The effect of composition on interfacial functionality was assessed by dilatational frequency and amplitude sweeps. Crude juice from asparagus stems formed weak interfaces with near linear viscoelastic behavior, whereas removal of particles and molecular impurities yielded stiffer interfaces that behaved highly nonlinear in large amplitude oscillations. The nonlinear responses were studied with Lissajous plots and a general stress decomposition method (de Groot et al., 2023). From the decomposition, we concluded that the removal of particles increased interfacial network stiffness and additional removal of small molecular components increased in-plane interactions even further, leading to a more dense interface, as shown for the filtered and purified extract.

Due to the improved interfacial properties, this filtered and purified extract was able to quickly form stable foams (due to the absence of particles and small molecular components). Compared to literature, foam overrun of the purified asparagus stem protein extract was comparable to other plant proteins.

With this study, we showed that asparagus stems are a potential source to produce protein extracts with good interfacial functionality and foaming properties, which can already be achieved by some relatively simple purification steps, such as filtration and dialysis. In further studies, it would be interesting to characterize the non-proteinaceous components, so conclusions can be drawn on how they affect network formation at the air-water interface. We showed that a multi-length scale approach is necessary for understanding the foaming characteristics of protein extracts. In this approach, the general stress decomposition identifies critical differences between interfacial properties of proteins that otherwise cannot be shown.

CRediT authorship contribution statement

Anteun de Groot: Conceptualization, Methodology, Investigation, Validation, Visualization, Writing – original draft. **Leonard M.C. Sagis:** Conceptualization, Methodology, Supervision, Writing – review & editing. **Jack Yang:** Conceptualization, Methodology, Investigation, Validation, Writing – review & editing.

Declaration of competing interest

The authors declare that they have no known competing financial interests or personal relationships that could have appeared to influence the work reported in this paper. This manuscript has not been published

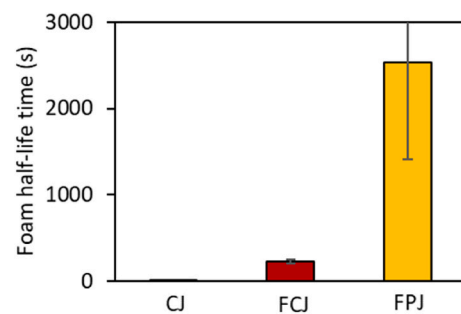


Fig. 10. The foam half-life time of CJ (blue), FCJ (red), and FPJ (yellow) measured in a Foamscan. The samples (50 mL, 0.1% w/w protein) were sparged until a foam volume of 400 cm³ was reached, then foam collapse was followed until the foam volume was halved.

and is not under consideration for publication in any other journal. All authors approve this manuscript and its submission to Food Hydrocolloids.

Data availability

Data will be made available on request.

Acknowledgements

This research did not receive any specific grant from funding agencies in the public, commercial, or not-for-profit sectors. We thank Joanne Siccama for advising and helping us obtain the Asparagus stems.

Appendix A. Supplementary data

Supplementary data to this article can be found online at <https://doi.org/10.1016/j.foodhyd.2023.109218>.

References

- Apaiiah, R. K., Linnemann, A. R., & Van Der Kooij, H. J. (2006). Exergy analysis: A tool to study the sustainability of food supply chains. *Food Research International*, 39(1), 1–11. <https://doi.org/10.1016/j.foodres.2005.04.006>
- Aveyard, R., Binks, B. P., Fletcher, P. D. I., Peck, T. G., & Rutherford, C. E. (1994). Aspects of aqueous foam stability in the presence of hydrocarbon oils and solid particles. *Advances in Colloid and Interface Science*, 48, 93–120. [https://doi.org/10.1016/0001-8686\(94\)80005-7](https://doi.org/10.1016/0001-8686(94)80005-7)
- Aveyard, R., & Clint, J. H. (1995). New method for the measurement of line tensions at the solid/liquid/air three-phase contact line. *Journal of the Chemical Society, Faraday Transactions*, 91(1), 175–176. <https://doi.org/10.1039/FT9959100175>
- Aveyard, R., & Clint, J. H. (1996). Particle wettability and line tension. *Journal of the Chemical Society Faraday Transactions*, 92(1), 85–89. <https://doi.org/10.1039/ft9969200085>
- Bergfreund, J., Bertsch, P., & Fischer, P. (2021). Adsorption of proteins to fluid interfaces: Role of the hydrophobic subphase. *Journal of Colloid and Interface Science*, 584, 411–417. <https://doi.org/10.1016/j.jcis.2020.09.118>
- Bolontrade, A. J., Scilingo, A. A., & Añón, M. C. (2013). Amaranth proteins foaming properties: Adsorption kinetics and foam formation-Part 1. *Colloids and Surfaces B: Biointerfaces*, 105, 319–327. <https://doi.org/10.1016/j.colsurfb.2012.12.039>
- Bos, M. A., & Van Vliet, T. (2001). Interfacial rheological properties of adsorbed protein layers and surfactants: A review. *Advances in Colloid and Interface Science*, 91(3), 437–471. [https://doi.org/10.1016/S0001-8686\(00\)00077-4](https://doi.org/10.1016/S0001-8686(00)00077-4)
- Chitrakar, B., Zhang, M., & Adhikari, B. (2019). Asparagus (*Asparagus officinalis*): Processing effect on nutritional and phytochemical composition of spear and hard-stem byproducts. *Trends in Food Science and Technology*, 93(5), 1–11. <https://doi.org/10.1016/j.tifs.2019.08.020>
- Clarkson, J. R., Cui, Z. F., & Darton, R. C. (1999). Protein denaturation in foam. *Journal of Colloid and Interface Science*, 215(2), 323–332. <https://doi.org/10.1006/jcis.1999.6255>
- Denkov, N. D., Marinova, K. G., & Tcholakova, S. S. (2014). Mechanistic understanding of the modes of action of foam control agents. *Advances in Colloid and Interface Science*, 206, 57–67. <https://doi.org/10.1016/j.cis.2013.08.004>. Elsevier B.V.
- Derbyshire, E., Wright, D. J., & Boulter, D. (1976). Legumin and vicilin, storage proteins of legume seeds. *Phytochemistry*, 15(1), 3–24. [https://doi.org/10.1016/S0031-9422\(00\)89046-9](https://doi.org/10.1016/S0031-9422(00)89046-9)
- Erni, P., & Parker, A. (2012). Nonlinear viscoelasticity and shear localization at complex fluid interfaces. *Langmuir*, 28(20), 7757–7767. <https://doi.org/10.1021/la301023k>

- Finkenstadt, V. L. (2014). A review on the complete utilization of the sugarbeet. *Sugar Technology*, 16(4), 339–346. <https://doi.org/10.1007/s12355-013-0285-y>
- Foastat. (2018). *Production quantity of Asparagus*. <http://www.fao.org/faostat/en/#data/QC>.
- Fruhner, H., Wantke, K.-D., & Lunkenheimer, K. (2000). Relationship between surface dilatational properties and foam stability. *Colloids and Surfaces A: Physicochemical and Engineering Aspects*, 162(1–3), 193–202. [https://doi.org/10.1016/S0927-7757\(99\)00202-2](https://doi.org/10.1016/S0927-7757(99)00202-2)
- Frye, G. C., & Berg, J. C. (1989). Mechanisms for the synergistic antifoam action by hydrophobic solid particles in insoluble liquids. *Journal of Colloid and Interface Science*, 130(1), 54–59. [https://doi.org/10.1016/0021-9797\(89\)90077-5](https://doi.org/10.1016/0021-9797(89)90077-5)
- Fuentes-Alventosa, J. M., Jaramillo-Carmona, S., Rodríguez-Gutiérrez, G., Guillén-Bejarano, R., Jiménez-Araujo, A., Fernández-Bolaños, J., et al. (2013). Preparation of bioactive extracts from asparagus by-product. *Food and Bioprocess Technology*, 91(2), 74–82. <https://doi.org/10.1016/j.fbp.2012.12.004>
- Garrett, P. R. (1979). The effect of polytetrafluoroethylene particles on the foamability of aqueous surfactant solutions. *Journal of Colloid and Interface Science*, 69(1), 107–121. [https://doi.org/10.1016/0021-9797\(79\)90085-7](https://doi.org/10.1016/0021-9797(79)90085-7)
- Geerts, M. E. J., Nikiforidis, C. V., van der Goot, A. J., & van der Padt, A. (2017). Protein nativity explains emulsifying properties of aqueous extracted protein components from yellow pea. *Food Structure*, 14(August), 104–111. <https://doi.org/10.1016/j.foosstr.2017.09.001>
- van der Goot, A. J., Pelgrom, P. J. M., Berghout, J. A. M., Geerts, M. E. J., Jankowiak, L., Hardt, N. A., et al. (2016). Concepts for further sustainable production of foods. *Journal of Food Engineering*, 168, 42–51. <https://doi.org/10.1016/j.jfoodeng.2015.07.010>
- Góral, I., & Wojciechowski, K. (2020). Surface activity and foaming properties of saponin-rich plants extracts. *Advances in Colloid and Interface Science*, 279. <https://doi.org/10.1016/j.cis.2020.102145>
- de Groot, A., Yang, J., & Sagis, L. M. C. (2023). Surface stress decomposition in large amplitude oscillatory interfacial dilatation of complex interfaces. *Journal of Colloid and Interface Science*, 638, 569–581. <https://doi.org/10.1016/j.jcis.2023.02.007>
- Ikedo, S., Shimoyamada, M., & Watanabe, K. (1996). Interaction between bovine serum albumin and saponin as studied by heat stability and protease digestion. *Journal of Agricultural and Food Chemistry*, 44(3), 792–795. <https://doi.org/10.1021/jf940742>
- Jaramillo-Carmona, S., Lopez, S., Vazquez-Castilla, S., Rodriguez-Arcos, R., Jimenez-Araujo, A., & Guillen-Bejarano, R. (2013). Asparagus byproducts as a new source of peroxidases. *Journal of Agricultural and Food Chemistry*, 61(26), 6167–6174. <https://doi.org/10.1021/jf4011609>
- Karaca, A. C., Low, N., & Nickerson, M. (2011). Emulsifying properties of chickpea, faba bean, lentil and pea proteins produced by isoelectric precipitation and salt extraction. *Food Research International*, 44(9), 2742–2750. <https://doi.org/10.1016/j.foodres.2011.06.012>
- Kawale, D., van Nimwegen, A. T., Portela, L. M., van Dijk, M. A., & Henkes, R. A. W. M. (2015). The relation between the dynamic surface tension and the foaming behaviour in a sparger setup. *Colloids and Surfaces A: Physicochemical and Engineering Aspects*, 481, 328–336. <https://doi.org/10.1016/j.colsurfa.2015.05.028>
- Lamsal, B. P., Koegel, R. G., & Gunasekaran, S. (2007). Some physicochemical and functional properties of alfalfa soluble leaf proteins. *LWT - Food Science and Technology*, 40(9), 1520–1526. <https://doi.org/10.1016/j.lwt.2006.11.010>
- Lee, E. J., Yoo, K. S., & Patil, B. S. (2010). Development of a rapid HPLC-UV method for simultaneous quantification of protodioscin and rutin in white and green Asparagus spears. *Journal of Food Science*, 75(9), 703–709. <https://doi.org/10.1111/j.1750-3841.2010.01824.x>
- L'Hocine, L., Boye, J. I., & Arcand, Y. (2006). Composition and functional properties of soy protein isolates prepared using alternative defatting and extraction procedures. *Journal of Food Science*, 71(3). <https://doi.org/10.1111/j.1365-2621.2006.tb15609.x>
- Lie-Piang, A., Braconi, N., Boom, R. M., & van der Padt, A. (2021). Less refined ingredients have lower environmental impact – a life cycle assessment of protein-rich ingredients from oil- and starch-bearing crops. *Journal of Cleaner Production*, 292, Article 126046. <https://doi.org/10.1016/j.jclepro.2021.126046>
- Lie-Piang, A., Yang, J., Schutysen, M. A. I., Nikiforidis, C. V., & Boom, R. M. (2023). Mild fractionation for more sustainable food ingredients. *Annual Review of Food Science and Technology*, 14(1), 473–493. <https://doi.org/10.1146/annurev-food-060721-024052>
- Lucassen, J., & Van Den Tempel, M. (1972). Dynamic measurements of dilatational properties of a liquid interface. *Chemical Engineering Science*, 27(6), 1283–1291. [https://doi.org/10.1016/0009-2509\(72\)80104-0](https://doi.org/10.1016/0009-2509(72)80104-0)
- Martínez, K. D., Carrera Sánchez, C., Rodríguez Patino, J. M., & Pilosof, A. M. R. (2009). Interfacial and foaming properties of soy protein and their hydrolysates. *Food Hydrocolloids*, 23(8), 2149–2157. <https://doi.org/10.1016/j.foodhyd.2009.03.015>
- Martin, A. H., Grolle, K., Bos, M. A., Cohen Stuart, M. A., & Van Vliet, T. (2002). Network forming properties of various proteins adsorbed at the air/water interface in relation to foam stability. *Journal of Colloid and Interface Science*, 254(1), 175–183. <https://doi.org/10.1006/jcis.2002.8592>
- Mitropoulos, V., Mütze, A., & Fischer, P. (2014). Mechanical properties of protein adsorption layers at the air/water and oil/water interface: A comparison in light of the thermodynamical stability of proteins. *Advances in Colloid and Interface Science*, 206, 195–206. <https://doi.org/10.1016/j.cis.2013.11.004>. Elsevier.
- Mohan, A., Nickerson, M. T., & Ghosh, S. (2020). Utilization of pulse protein-xanthan gum complexes for foam stabilization: The effect of protein concentrate and isolate at various pH. *Food Chemistry*, 316(April 2019), Article 126282. <https://doi.org/10.1016/j.foodchem.2020.126282>
- Oleszek, M., & Oleszek, W. (2020). Saponins in food. In *Handbook of dietary phytochemicals* (pp. 1–40). Springer Singapore. https://doi.org/10.1007/978-981-13-1745-3_34-1.
- Ozdal, T., Capanoglu, E., & Altay, F. (2013). A review on protein-phenolic interactions and associated changes. *Food Research International*, 51(2), 954–970. <https://doi.org/10.1016/j.foodres.2013.02.009>
- Pegiou, E., Siccamo, J. W., Mumm, R., Zhang, L., Jacobs, D. M., Lauteslager, X. Y., et al. (2023). Metabolomics and sensory evaluation of white asparagus ingredients in instant soups unveil important (off-)flavours. *Food Chemistry*, 406, Article 134986. <https://doi.org/10.1016/j.foodchem.2022.134986>
- Ralla, T., Salminen, H., Edelmann, M., Dawid, C., Hofmann, T., & Weiss, J. (2017). Sugar beet extract (Beta vulgaris L.) as a new natural emulsifier: Emulsion formation. *Journal of Agricultural and Food Chemistry*, 65(20), 4153–4160. <https://doi.org/10.1021/acs.jafc.7b00441>
- Richtering, W. (2012). Responsive emulsions stabilized by stimuli-sensitive microgels: Emulsions with special non-pickering properties. *Langmuir*, 28(50), 17218–17229. <https://doi.org/10.1021/la302331s>
- Roberts, K., Axberg, C., & Österlund, R. (1977). The effect of spontaneous emulsification of defoamer on foam prevention. *Journal of Colloid and Interface Science*, 62(2), 264–271. [https://doi.org/10.1016/0021-9797\(77\)90120-5](https://doi.org/10.1016/0021-9797(77)90120-5)
- Rodríguez, R., Jaramillo, S., Guillén, R., Jiménez, A., Fernández-Bolaños, J., & Heredia, A. (2005). Cell wall phenolics of white and green asparagus. *Journal of the Science of Food and Agriculture*, 85(6), 971–978. <https://doi.org/10.1002/jsfa.2053>
- Rodríguez, R., Jaramillo, S., Rodríguez, G., Espejo, J. A., Guillén, R., Fernández-Bolaños, J., et al. (2005). Antioxidant activity of ethanolic extracts from several Asparagus cultivars. *Journal of Agricultural and Food Chemistry*, 53(13), 5212–5217. <https://doi.org/10.1021/jf050338i>
- Rühs, P. A., Affolter, C., Windhab, E. J., & Fischer, P. (2013). Shear and dilatational linear and nonlinear subphase controlled interfacial rheology of β -lactoglobulin fibrils and their derivatives. *Journal of Rheology*, 57(3), 1003–1022. <https://doi.org/10.1122/1.4802051>
- Sagis, L. M. C., Liu, B., Li, Y., Essers, J., Yang, J., Moghimikheirabadi, A., et al. (2019). Dynamic heterogeneity in complex interfaces of soft interface-dominated materials. *Scientific Reports*, 9(1), 1–12. <https://doi.org/10.1038/s41598-019-39761-7>
- Shevkani, K., Singh, N., Kaur, A., & Rana, J. C. (2015). Structural and functional characterization of kidney bean and field pea protein isolates: A comparative study. *Food Hydrocolloids*, 43, 679–689. <https://doi.org/10.1016/j.foodhyd.2014.07.024>
- Tanaka, M., Fang, I.-L., Ishizaki, S., & Taguchi, T. (1995). Interaction of saponins with salt soluble proteins from walleye pollack meat. *Fisheries Science*, 61(2), 373–374. <https://doi.org/10.2331/fishsci.61.373>
- Urbat, F., Müller, P., Hildebrand, A., Wefers, D., & Bunzel, M. (2019). Comparison and optimization of different protein nitrogen quantitation and residual protein characterization methods in dietary fiber preparations. *Frontiers in Nutrition*, 6 (August), 1–8. <https://doi.org/10.3389/fnut.2019.00127>
- Van Kempen, S. E. H. J., Schols, H. A., Van Der Linden, E., & Sagis, L. M. C. (2013). Non-linear surface dilatational rheology as a tool for understanding microstructures of air/water interfaces stabilized by oligofructose fatty acid esters. *Soft Matter*, 9(40), 9579–9592. <https://doi.org/10.1039/c3sm51770e>
- Wang, M., Tadmor, Y., Wu, Q. L., Chin, C. K., Garrison, S. A., & Simon, J. E. (2003). Quantification of protodioscin and rutin in asparagus shoots by LC/MS and HPLC methods. *Journal of Agricultural and Food Chemistry*, 51(21), 6132–6136. <https://doi.org/10.1021/jf0344587>
- Wang, H., van den Berg, F. W. J., Zhang, W., Czaja, T. P., Zhang, L., Jespersen, B. M., et al. (2022). Differences in physicochemical properties of high-moisture extrudates prepared from soy and pea protein isolates. *Food Hydrocolloids*, 128. <https://doi.org/10.1016/j.foodhyd.2022.107540>
- Wierenga, P. A., Meinders, M. B. J., Egmond, M. R., Voragen, F. A. G. J., & De Jongh, H. H. J. (2003). Protein exposed hydrophobicity reduces the kinetic barrier for adsorption of ovalbumin to the air-water interface. *Langmuir*, 19(21), 8964–8970. <https://doi.org/10.1021/la034868p>
- Yang, J., Kornet, R., Diedericks, C. F., Yang, Q., Berton-Carabin, C. C., Nikiforidis, C. V., et al. (2022). Rethinking plant protein extraction: Albumin—from side stream to an excellent foaming ingredient. *Food Structure*, 31. <https://doi.org/10.1016/j.foosstr.2022.100254>
- Yang, J., Mocking-Bode, H. C. M., van den Hoek, I. A. F., Theunissen, M., Voudouris, P., Meinders, M. B. J., et al. (2022). The impact of heating and freeze or spray drying on the interface and foam stabilising properties of pea protein extracts: Explained by aggregation and protein composition. *Food Hydrocolloids*, 133. <https://doi.org/10.1016/j.foodhyd.2022.107913>
- Yu, Q., Duan, J., Yu, N., & Fan, L. (2020). Enhancing the antityrosinase activity of saponins and polyphenols from Asparagus by hot air coupled with microwave treatments. *Lwt*, 124(October 2019), Article 109174. <https://doi.org/10.1016/j.lwt.2020.109174>
- Zhang, C., Sanders, J. P. M., & Bruins, M. E. (2014). Critical parameters in cost-effective alkaline extraction for high protein yield from leaves. *Biomass and Bioenergy*, 67, 466–472. <https://doi.org/10.1016/j.biombioe.2014.05.020>, 0.